Available online at www.sciencedirect.com
SCIENCE DIRECT®
International Journal of Mass Spectrometry 243 (2005) 205–214
International Journal of Mass Spectrometry
www.elsevier.com/locate/ijms

Mass spectral and theoretical characterisation of non-symmetric Mo(V) dithiolene complexes

Hélène Lavanant [a,*], Catherine Fressigné [a], Corine Simonnet-Jégat [b], Rémi Dessapt [b], Alain Mallard [b], Francis Sécheresse [b], Nicole Sellier [c]

[a] *Department of Chemistry, Institut de Recherche en Chimie Organique Fine, UMR CNRS 6014, Université de Rouen, 76821 Mont St Aignan, France*
[b] *Institut Lavoisier, UMR CNRS 8637, Université de Versailles-St-Quentin, 45 Avenue des Etats-Unis, 78035 Versailles, France*
[c] *Laboratoire de Synthèse Organique Sélective et Produits Naturels, CNRS, UMR 7573, Ecole Nationale Supérieure de Chimie de Paris, 11 Rue Pierre et Marie Curie, 75231 Paris Cedex 05, France*

Received 10 December 2004; accepted 7 March 2005
Available online 9 April 2005

Abstract

The gas phase fragmentations of a family of three anionic complexes of molybdenum(V), $[Mo_2(O)_2(\mu\text{-}S)_2(\eta^2\text{-}S_2)_2]^{2-}$, $[Mo_2(O)_2(\mu\text{-}S)_2(\eta^2\text{-}S_2)(\eta^2\text{-}S_2C_2H_2)]^{2-}$, $[Mo_2(O)_2(\mu\text{-}S)_2(\eta^2\text{-}S_2)(\eta^2\text{-}S_2C_2(C_6H_5)_2)]^{2-}$ were studied as a function of the collision energy used in the collision cell of a triple quadrupole analyser. The main fragment ion for the three anions was $Mo_2S_4O_2^-$ at low collision energies, while higher collisional activation led to cleavage of the "metal–metal" bond. Topological analyses of the electronic domains using the electron localisation function (ELF) showed that non-symmetric fragmentation behaviour could be interpreted according to the least topological change principle. Fragmentation induced a slight shift of the electron density towards the remaining ligands and an increase of the electron population on the Mo atom that undergoes a decrease of its coordination sphere.

Keywords: Energy-resolved mass spectrometry; Electrospray ionisation; DFT calculations; Electron ELF analysis; Mo(V) dithiolene complexes

1. Introduction

Electrospray mass spectrometry (ESI MS) now allows the production of gas phase inorganic ions from polar solutions in which they are soluble [1]. In fact, mass spectra have been obtained for a variety of inorganic and organometallic compounds ranging from coordination compounds [2] to metallocene derivatives [3], to metal clusters [4] and supramolecular complexes [5]. Electrospray mass spectrometry as well as matrix-assisted laser desorption ionisation (MALDI) thus opens new possibilities for structural analysis in inorganic chemistry. One of these possibilities is the investigation of the gas phase chemistry of a family of compounds rather new to the field of mass spectrometry. Although the study of gas phase fragmentation of ions by mass spectrometry has long been established as a valuable technique for structural characterisation of organic compounds and biopolymers, to our knowledge however, few studies [6] have been devoted to the gas phase fragmentations of complex inorganic ions produced by electrospray.

Dithiolene complexes of molybdenum(V) have recently attracted considerable attention because they may be used to model the active site of ubiquitous molybdenum enzymes [7]. Non-symmetric dinuclear complexes are also a particular object of interest as they should show unusual catalytic and redox chemistry due to a polarised metal–metal bond and non-symmetric coordination spheres [8,9].

Synthesis of such compounds involves addition of electrophiles on tetraoxothiomolybdates [10,11] and yields a large diversity of new sulphur rich compounds, which, in some cases, are produced as mixtures. Consequently, pure crystals are sometimes very difficult to obtain and X-ray crystallography cannot always be used. Electrospray mass

* Corresponding author. Tel.: +33 2 35 52 29 32; fax: +33 2 35 52 24 41.
E-mail address: helene.lavanant@univ-rouen.fr (H. Lavanant).

1387-3806/$ – see front matter © 2005 Elsevier B.V. All rights reserved.
doi:10.1016/j.ijms.2005.03.002

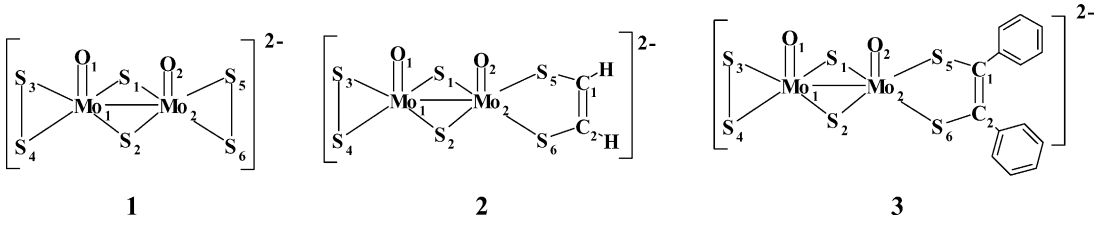

Scheme 1.

spectrometry therefore comes as a reliable and straightforward means of analysis: the mass over charge ratio and typical isotopic distribution of the intact complex anions provide sufficient information for an assignment of the molecular formula of the compounds.

This particular piece of information, however, is only a fraction of what is available in the mass spectra. Indeed, in addition to the intact complexes, a variety of fragment ions can be found whose formulae depend on the structure of the precursor ion and on the energy of the ions in the nozzle-skimmer area of the electrospray source.

The objectives of this work was to investigate the gas phase fragmentations of a group of three anionic complexes of molybdenum(V) (Scheme 1) that all include a common dinuclear *syn*-$[Mo_2(O)_2(\mu\text{-}S)_2]$ core. Although many compounds comprising this core exist, they all entail identical ligands, and non-symmetric dinuclear complexes are quite rare [12]. Our purpose was therefore to achieve new insights on the gas phase behaviour of these complexes. This was done as a function of the collision energy used in the collision cell of a triple quadrupole analyzer, with a focus on the effect of the differentiated ligands.

With this energy-resolved mass spectrometry, a thorough characterisation of the gas phase fragmentation pathways of closely related compounds can be achieved. Dissociation patterns can thus be delineated with the objective to be able to use this knowledge in the future to help distinguish isomers in new syntheses. To further interpret observed gas phase fragmentations and relate our energy-resolved data to the structures of the precursor ions, molecular calculations were carried out, including topological analyses of the electronic domain using the electron localisation function (ELF) [13].

2. Materials and methods

2.1. Materials

Preparation of the three molybdenum(V) complexes, $(N(C_2H_5)_4)_2$ $[Mo_2(O)_2(\mu\text{-}S)_2(\eta^2\text{-}S_2)_2]$ **1**, $(N(C_2H_5)_4)_2$ $[Mo_2(O)_2(\mu\text{-}S)_2(\eta^2\text{-}S_2)$ $(\eta^2\text{-}S_2C_2H_2)]$ **2**, $(N(C_2H_5)_4)_2$ $[Mo_2(O)_2(\mu\text{-}S)_2(\eta^2\text{-}S_2)(\eta^2\text{-}S_2C_2(C_6H_5)_2)]$ **3** is described elsewhere [10,11]. Solutions (10^{-4} mol L^{-1}) were prepared from pure acetonitrile (J.T. Baker), which was used as received without additional purification.

2.2. Mass spectrometry

Mass spectral measurements were carried out with an API 3000 (ESI MS/MS) Applied Biosystems triple quadrupole mass spectrometer. The instrument was operated in the negative ion mode. The experiments were performed by direct infusion with a syringe pump with a flow rate of 5 μL min^{-1}. Standard experimental conditions were as follows: sample concentration, (2–4) × 10^{-4} mol L^{-1}; nebulizing gas N_2, 7 units flow rate; ion spray voltage, −5.00 kV; temperature, 150 °C; declustering potential, −20 V; focusing potential, −200 V; entrance potential, 10 V. The mass spectra shown are the result of approximately 20 scans summed from *m*/*z* 20 to 600. The mass axis was externally calibrated using standard calibrants.

For MS/MS experiments, N_2 was used as collision gas, and pressure was adjusted so as to obtain 30% attenuation of the precursor ion at the lowest energy (5 eV). Standard unit resolution was used for the mass selection of the precursor ions, the center mass being the most abundant isotopic combination. The total isotopic distribution being spread over 7 *m*/*z* units for our doubly-charged precursor ions, only three or four of the most abundant isotopic combination were selected and the full isotopic pattern was therefore lost upon selection. Collision energy was ramped stepwise (step, −1 V) from 5 to 30 or 40 V, the ramp was carried out over a 10 min period so as to allow sufficient data points at every different energy. Resolving power was set so as to achieve standard unit resolution.

2.3. Computational method

Calculations were performed with the Gaussian 98 program [14], using the hybrid density Functional B3LYP [15,16] method. It has been recently proved that accurate values of structural properties can be obtained with method for second row transition metal dinuclear complexes [17].

All calculations have been performed using the “DZVP” basis [18] set for Mo, C and H atoms but it appeared necessary to add diffuse functions on S and O atoms.

The ELF calculations were carried out with the TopMod package developed at the Laboratoire de Chimie Théorique de L’Université Pierre & Marie Curie [19]. Isosurfaces have been visualized with the public domain scientific visualization and animation program for high performance graphic workstations named SciAn [20].

3. Results and discussion

3.1. Fragmentation of $[Mo_2(O)_2(\mu\text{-}S)_2(\eta^2\text{-}S_2)_2]^{2-}$

The electrospray mass spectrum of $(N(C_2H_5)_4)_2$ $[Mo_2(O)_2(\mu\text{-}S)_2(\eta^2\text{-}S_2)_2]$ **1** is shown in Fig. 1. At low cone voltages, the expected signal of the anion **1** was observed at *m*/*z* 208 (most abundant isotopic combination) with an isotopic distribution very similar to the predicted profile (see inset in Fig. 1). The chosen resolution, even when set to standard unit resolution, therefore allowed to distinguish individual isotopic peaks both for doubly and singly charged ions. The isotopic distributions displayed by the other peaks observed on the mass spectrum thus allowed an assignment to species containing two Mo atoms. The base peak of the mass spectrum at *m*/*z* 352.1 corresponded to a $Mo_2S_4O_2^-$ anion. This formula obviously indicated it was a fragment ion of **1** in which a S_2^- group was lost. This S_2^- fragment is in fact a radical anion, formally making this fragmentation an intramolecular redox reaction, which can be related to the generation of amino acid and peptide radicals by collision activation of amino acid and peptide metal complexes [21]. Loss of radical anion as oxidized dithiolate $S_2C_2(CN)_2^-$ has also been reported by Waters et al. [22] from the anionic complexes $[MoO_2(S_2C_2(CN)_2]^{2-}$ and $[WO_2(S_2C_2(CN)_2]^{2-}$.

Another abundant distribution in the electrospray mass spectrum was assigned to the parent anion associated with a tetraethyl ammonium counter ion $[Mo_2S_6O_2, N(C_2H_5)_4]^-$. The lower intensity peaks around *m*/*z* 368 and 384 could be attributed to $Mo_2S_xO_y^-$ ($x = 5, 6$; $y = 1, 0$) type complexes where one or two of the terminal oxygen atoms of $Mo_2S_4O_2^-$ were replaced by sulphurs or the reverse. These minor components were correlated to traces of $Mo_2S_xO_y^{2-}$ ($x = 7, 8$; $y = 1, 0$) at *m*/*z* 216 and 224, expected to be present as a result of the synthesis, as the main reagent MoS_3O^- contained low proportions of $MoS_2O_2^-$, MoS_4^- and $MoSO_3^-$. Finally, the peaks at *m*/*z* 240 and 416 were attributable to the formal addition of two sulphur atoms to $Mo_2S_6O_2^{2-}$ and $Mo_2S_4O_2^-$, respectively.

To further investigate the fragmentation processes undergone by anion **1**, a collection of product ion spectra at different collision energies were recorded. As expected, the nature and relative intensities of the product ions of precursor ion **1** were found to depend on the collision energy as shown in Fig. 2. Low collision energies (Fig. 2a: 10 eV) yielded product mass spectra showing essentially the $Mo_2S_4O_2^-$ fragment and its complementary S_2^- ion; while high collision energies (Fig. 2b: 30 eV) induced the appearance of a collection of fragment ions with only one Mo atom: $MoS_xO_y^-$ ($x = 1$–3; $y = 1, 2$). Note that, as only a few of the most abundant isotopic ions were selected, the full isotopic pattern was lost. However, one could easily distinguish doubly charged ions such as precursor ion $Mo_2S_6O_2^{2-}$ or fragment ion $Mo_2S_4O_2^{2-}$ from singly charged fragment ions with similar *m*/*z* values MoS_3O^- and MoS_2O^- from the larger spread and shape of the isotopic distribution with peaks spaced 1 *m*/*z* unit apart. We summarized this data on the breakdown graph displayed on Fig. 3, which represents a plot of the ion abundance as a percentage of the total ion current versus the collision energy in the laboratory frame E_{lab}. At low collision energies, precursor ion $Mo_2S_6O_2^{2-}$ was observed but never found as the most abundant ion. It was thus confirmed that the fragmentation yielding $Mo_2S_4O_2^{2-}$ required very little energy. At higher collision energies (25 eV), the metal–metal bond

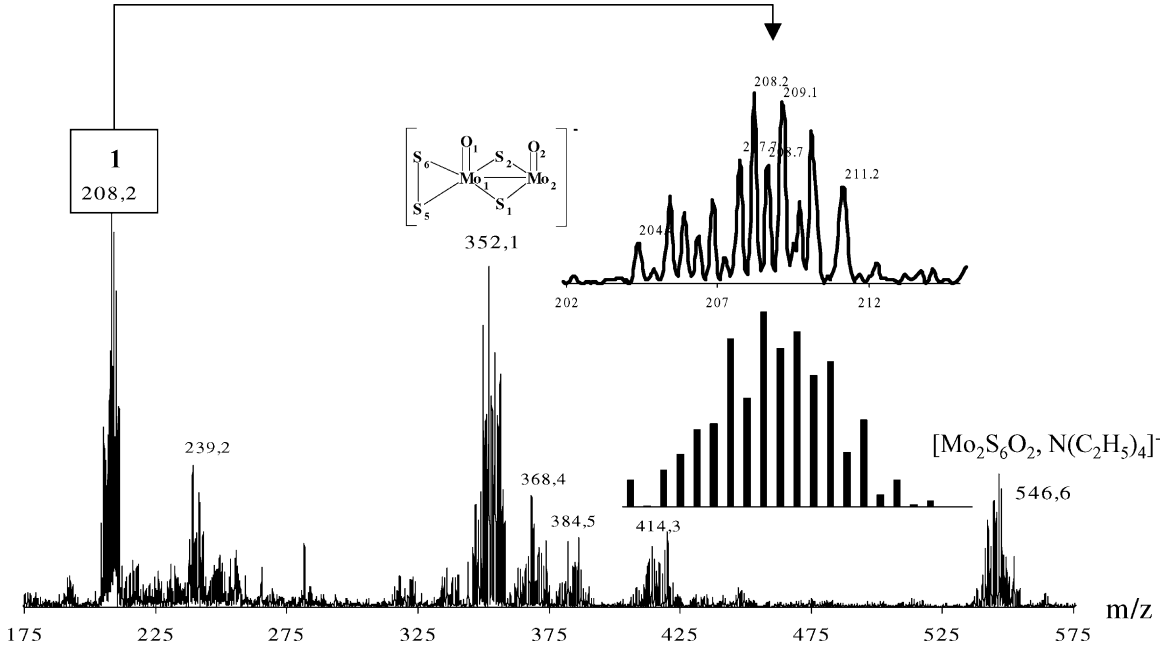

Fig. 1. Negative ion mode electrospray mass spectrum of $(N(C_2H_5)_4)_2$ $[Mo_2(O)_2(\mu\text{-}S)_2(\eta^2\text{-}S_2)_2$ (2×10^{-5} mol L^{-1} in acetonitrile). The inset shows an expanded view of $[Mo_2(O)_2(\mu\text{–}S)_2(\eta^2\text{–}S_2)_2]^{2-}$ compared to the theoretical isotopic distribution.

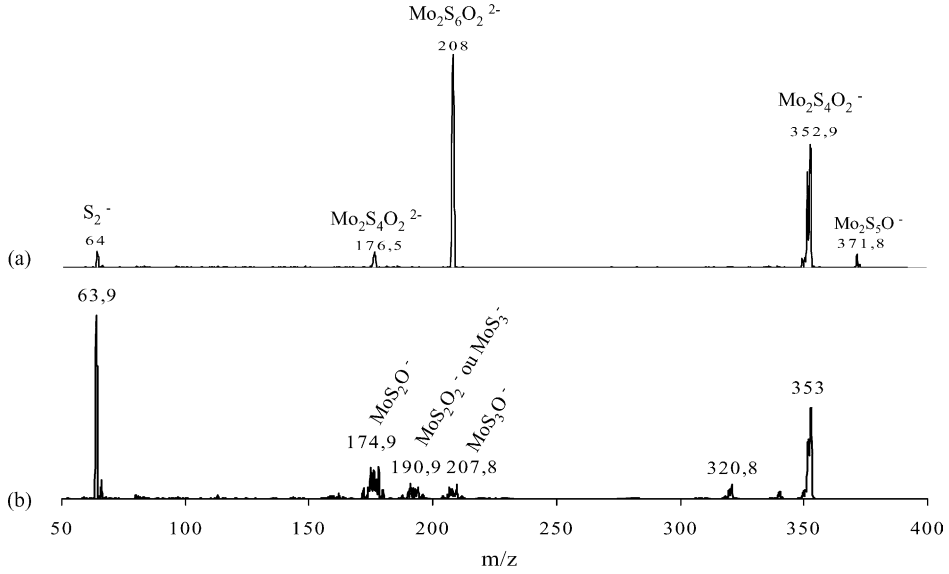

Fig. 2. Product ion mass spectra of **1** $[Mo_2(O)_2(\mu\text{–}S)_2(\eta^2\text{–}S_2)_2]^{2-}$ (*m*/*z* 208) at different collision energies: (a) E_{lab} = 10 eV and (b) E_{lab} = 30 eV.

was broken yielding a series of singly charged ions containing only one Mo atom. For clarity only the most abundant mononuclear anion MoS_2O^- is represented.

3.2. *Fragmentation of* $[Mo_2(O)_2(\mu\text{-}S)_2(\eta^2\text{-}S_2)(\eta^2\text{-}S_2C_2H_2)]^{2-}$ *and* $[Mo_2(O)_2(\mu\text{-}S)_2(\eta^2\text{-}S_2)(\eta^2\text{-}S_2C_2(C_6H_5)_2)]^{2-}$

For $(N(C_2H_5)_4)_2$ $[Mo_2(O)_2(\mu\text{-}S)_2(\eta^2\text{-}S_2)$ $(\eta^2\text{-}S_2C_2H_2)]$ **2**, $(N(C_2H_5)_4)_2$ $[Mo_2(O)_2(\mu\text{-}S)_2(\eta^2\text{-}S_2)(\eta^2\text{-}S_2C_2(C_6H_5)_2)]$ **3**, electrospray mass spectra were quite similar to that of **1**: along with the expected peaks at *m*/*z* 221 and 298 (most abundant isotope), attributed to **2** and **3**, a similar signal at *m*/*z* 351.7 from $Mo_2S_4O_2^-$ was observed (data not shown). This suggested the fragmentation was similar to that of **1** for both compounds. Notably, however, in these non-symmetric complexes, only the dithiolene ligand was lost and no trace of S_2^- loss was observed. The complementary ions $Mo_2S_4O_2C_2H_2^-$ and $Mo_2S_4O_2C_2(C_6H_5)_2^-$ were not observed either.

This non-symmetric fragmentation behaviour was observed at all collision energies. Breakdown graphs for **2** and **3** following the same protocol as for **1** (Figs. 4 and 5) showed that at low collision energies, the precursor ions remained intact. Upon an increase of the collision energy, $Mo_2S_4O_2^-$ anion could be observed along with the complementary fragment ions $S_2C_2H_2^-$, and $S_2C_2(C_6H_5)_2^-$. The highest

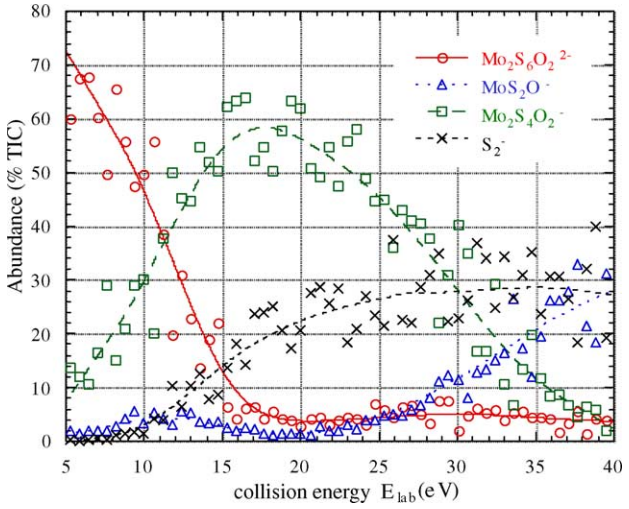

Fig. 3. Breakdown graph of **1** $[Mo_2(O)_2(\mu\text{–}S)_2(\eta^2\text{–}S_2)_2]^{2-}$. Abundances are percentages of the total ion current (TIC), the collision energy is in the laboratory referential (E_{lab}). For clarity, only one out of 20 data points is shown and the curves represent the 20% weighted curve fits.

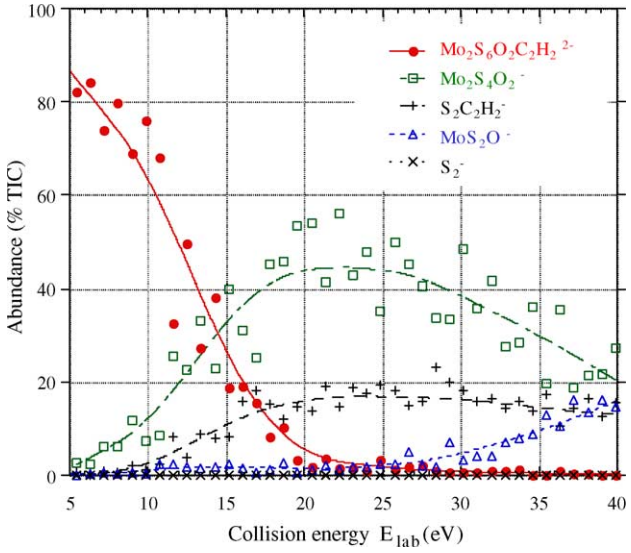

Fig. 4. Breakdown graph of **2** $[Mo_2(O)_2(\mu\text{-}S)_2(\eta^2\text{-}S_2)$ $(\eta^2\text{-}S_2C_2H_2)]^{2-}$. Abundances are percentages of the total ion current (TIC), the collision energy is in the laboratory referential (E_{lab}). For clarity, only one out of 20 data points is shown and the curves represent the 20% weighted curve fits.

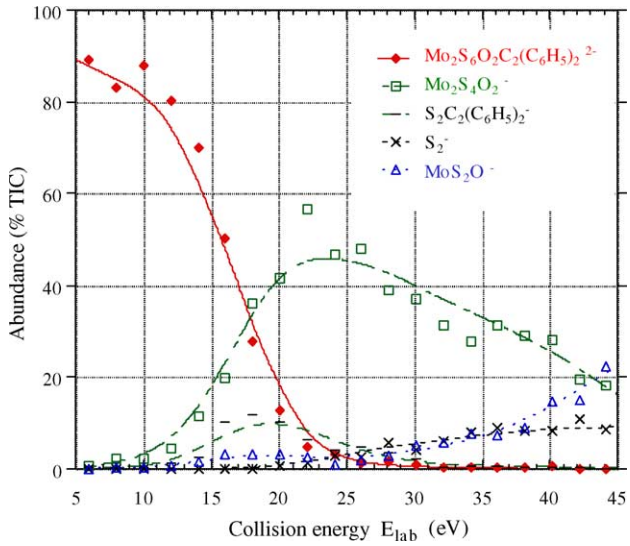

Fig. 5. Breakdown graph of **3** $[Mo_2(O)_2(\eta\text{-}S)_2(\eta^2\text{-}S_2)(\eta^2\text{-}S_2C_2(C_6H_5)_2)]^{2-}$. Abundances are percentages of the total ion current (TIC), the collision energy is in the laboratory referential (E_{lab}). For clarity, only one out of 30 data points is shown and the curves represent the 20% weighted curve fits.

collision energy allowed cleavage of the metal–metal bond resulting in several anions involving one Mo atom.

The breakdown curves for precursor ions 1–3 are compared in Fig. 6. This graph, represented as a function of the energy in the center of mass frame E_{CM}, shows a discrepancy of about 0.1 eV between the curves of **2** and **3** and that of **1**. The latter reached a 50% fragmentation ratio for a value of 0.6 eV while the other precursor ions attained this value at about 0.7 eV, with a steeper slope for **2**. Dissociation energies for compounds **2** and **3** are thus expected to be lower than that of compound **1** although in all three cases the main fragment ion $Mo_2S_4O_2^-$ is the same.

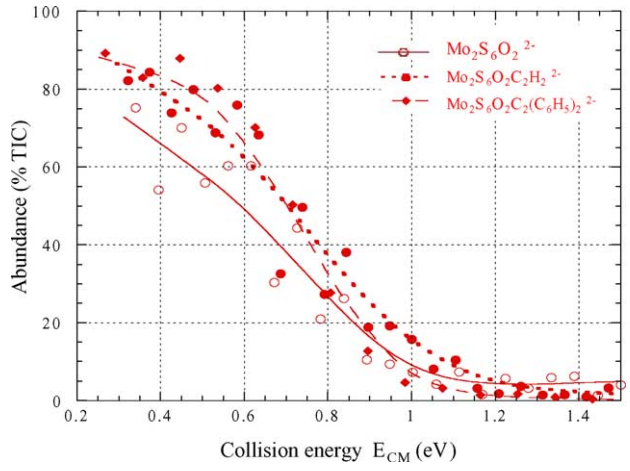

Fig. 6. Compared breakdown curves of precursor ions **1** (open circles, full line) **2** (full circles, dotted line) and **3** (diamonds, dashed line). Abundances are percentages of the total ion current (TIC), the collision energy is in the centre of mass referential (E_{CM}). For clarity, only one out of 30 data points is shown and the curves represent the 20% weighted curve fits.

3.3. Computational results

To further interpret these gas phase fragmentations and in particular seak an interpretation to the non-symmetric behaviour of compounds **2** and **3**, molecular calculations were carried out. Experimental data on the geometries of the three anions studied were available as crystallographic data were obtained for the three compounds $(N(C_2H_5)_4)_2$ $[Mo_2(O)_2(\mu\text{-}S)_2(\eta^2\text{-}S_2)_2]$ **1**, $(N(C_2H_5)_4)_2$ $[Mo_2(O)_2(\mu\text{-}S)_2(\eta^2\text{-}S_2)(\eta^2\text{-}S_2C_2H_2)]$ **2**, $(N(C_2H_5)_4)_2$ $[Mo_2(O)_2((\mu\text{-}S)_2(\eta^2\text{-}S_2)(\eta^2\text{-}S_2C_2(C_6H_5)_2)]$ **3** from a previous study [10,11]. Crystallographic data could therefore be used both as a starting point and to validate the choices for basis and density functional of our DFT calculations. To complete our understanding of the different chemical bonds and electronic distribution in the three compounds and the main fragment ion $Mo_2S_4O_2^-$, topological analyses of the electronic domain using the electron localisation function [13] were then carried out.

3.3.1. Geometry optimisations

Experimental parameters from the crystallographic structures of compounds $(N(C_2H_5)_4)_2$ $[Mo_2(O)_2(\mu\text{-}S)_2(\eta^2\text{-}S_2)(\eta^2\text{-}S_2C_2H_2)]$ **2**, $(N(C_2H_5)_4)_2$ $[Mo_2(O)_2(\mu\text{-}S)_2(\eta^2\text{-}S_2)(\eta^2\text{-}S_2C_2(C_6H_5)_2)]$ **3** [10,11] were used as starting point for the DFT geometry optimisations. In absence of information on the multiplicity of the complexes, several values (1, 2 and 6) were tested. In all cases, the closed-shell configuration was found lower in energy. Frequency calculations were carried out and all stationary points obtained were found to be local or most likely global minima of the potential energy surface. The energies of the optimized geometries (including zero point vibrational energies) for the three precursor ions **1**, **2** and **3** and several fragment ions are collected in Table 1. Among these fragment ions only $Mo_2S_4O_2^-$, S_2^-, $S_2C_2H_2^-$ and $S_2C_2(C_6H_5)_2^-$ were observed in significant amounts. For information, three other fragment ions were also calculated. Fragment ion MoS_3O^- that would correspond to a symmetric cleavage of the metal–metal bond, was observed only with a very low intensity. Fragment ions $[Mo_2(O)_2(\mu\text{-}S)_2(\eta^2\text{-}S_2C_2H_2)]^-$, and $[Mo_2(O)_2(\mu\text{-}S)_2(\eta^2\text{-}S_2C_2(C_6H_5)_2)]^-$ which would correspond to the loss of S_2^- from complexes **2** and **3** were totally unobserved. For all structures, zero point vibrational energies were found not to alter the relative stability order of any of the entities calculated.

From these values, the energies of the endothermic dissociation of our precursor anions to the fragment ion $Mo_2S_4O_2^-$ could be calculated: 1.1, 1.7 and 1.4 eV were found for **1**, **2** and **3**, respectively. These values confirm the precursor ions were indeed easily fragmented and that the complexes bearing dithiolene ligands required a slightly higher amount of energy to dissociate. While the order of magnitude was consistent, the experimental values observed appeared lower. Such values, however, could not be considered as exact with an instrument not devoted to threshold measurements.

Table 1
Energies of the optimised geometries for the three precursor ions **1**, **2** and **3** and several fragment ions

Formulae (low spin configuration)	Sum of electronic and zero point energies (a.u.)	Zero point vibrational energy (a.u.)
$[Mo_2(O)_2(\mu\text{-}S)_2(\eta^2\text{-}S_2)_2]^{2-}$ **1**	−10494.201766	0.016616
$[Mo_2(O)_2(\mu\text{-}S)_2(\eta^2\text{-}S_2)\ (\eta^2\text{-}S_2C_2H_2)]^{2-}$ **2**	−10571.579699	0.048877
$[Mo_2(O)_2(\mu\text{-}S)_2(\eta^2\text{-}S_2)(\eta^2\text{-}S_2C_2(C_6H_5)_2)]^{2-}$ **3**	−11033.565909	0.031380
$Mo_2S_4O_2^-$	−9697.789930	0.013486
S_2^-	−796.370912	0.001223
$S_2C_2H_2^-$	−873.726287	0.048877
$S_2C_2(C_6H_5)^-$	−1335.724111	0.193747
$[Mo_2(O)_2(\mu\text{-}S)_2(\eta^2\text{-}S_2C_2H_2)]^-$	−9775.208302	0.045858
$[Mo_2(O)_2\ (\mu\text{-}S)_2(\eta^2\text{-}S_2\ C_2(C_6\ H_5)_2)]^-$	−10237.200172	0.206875
MoS_3O^-	−5247.098687	0.00717

Other hypothetical dissociations of the precursor ions could also be evaluated. Surprisingly, the symmetric cleavage of the metal–metal bond yielding MoS_3O^- from ionic complex **1**, was found to require only 0.2 eV! Similarly, loss of S_2^- from precursor ions with dithiolene ligands was reckoned at 0.01 eV for complex **2** or to be exothermic by 0.1 eV for complex **3**! Obviously, transition states should play an important role to explain why these reactions remain unobserved and why the cleavage yielding $Mo_2S_4O_2^-$ is very largely the dominant process. Unfortunately, our repeated attempts to calculate these transition states have remained unsuccessful until now.

For ionic complexes **1**, **2** and **3**, DFT calculations could be validated by comparison of optimised and experimental parameters (Table 2). This comparison showed slightly shorter interatomic distances for the crystallographic geometry. The Mo–Mo distance was found to be 2.89 Å in the optimized structure compared to a 2.83 Å experimental value. Similarly, Mo–S and Mo–O distances were found 0.10–0.05 Å longer in the computed structure. This is consistent with the fact that crystallographic data is obtained in the solid state and in presence of a counter ion whereas the computed structures model intrinsic geometries in the gas phase and without any counter ion, which should be applicable in our mass spectrometric study. Otherwise, the general shapes of the experimental and computed structures were largely identical.

The compared geometries of the three precursor anions showed few differences. The principal change concerned the Mo–S distances of the two molybdenum atoms and the two bridging sulfido groups, which appeared shorter on the side of terminal disulfide ligand. This change appears as well on the crystallographic data [10,11] and is probably due to the presence of two different types of terminal ligands. No significant difference was observed in the parameters involving the terminal disulfide ligand, and the terminal oxygen atoms. This conserved geometry was also largely true for the fragment ion $Mo_2S_4O_2^-$ for which the Mo–Mo distance was found slightly shorter. A distortion of the *syn*-$[Mo_2(O)_2(\mu\text{-}S)_2]$ core was also observed: the Mo–S distances of the tricoordinated molybdenum atom was found slightly shorter

Table 2
Selected excerpt of the optimised and experimental structural parameters (distances in Å, angles in degrees) for the three precursor ions **1**, **2** and **3** and the main fragment ion $Mo_2S_4O_2^-$

	1		**2**		**3**		$Mo_2S_4O_2^-$
	Calculated	Experimental	Calculated	Experimental	Calculated	Experimental	Calculated
Mo_1–Mo_2	2.89	2.83	2.92	2.84	2.92	2.83	2.85
Mo_1–S_3	2.50	2.40	2.48	2.40	2.47	2.40	2.43
S_3–S_4	2.13	2.07	2.13	2.06	2.13	2.06	2.12
Mo_1–O_1	1.71	1.67	1.67	1.69	1.72	1.68	1.70
Mo_2–O_2	1.71	1.67	1.67	1.69	1.72	1.68	1.74
Mo_1–S_1	2.37	2.32	2.35	2.31	2.35	2.30	2.43
Mo_2–S_1	2.37	2.32	2.40	2.35	2.40	2.35	2.28
Mo_1–S_1–Mo_2	75	75	75	75	76	75	74
Mo_1–Mo_2–O_2	105	107	107	105	104	110	108; 131
Mo_2–Mo_1–S_3	137	134	134	136	137	135	132
S_3–Mo_1–S_4	51	51	51	51	51	51	52
S_1–Mo_1–S_2	102	102	102	102	99	102	99; 109
S_5–Mo_2–S_6	51	51	81	81	80	80	n.a.
Mo_1–Mo_2–S_5	137	137	130	128	130	127	n.a.
O_1–Mo_1–Mo_2–O_2	0	1	0	1	0	5	0
S_3–Mo_1–Mo_2–S_5	0	0	18	17	0	18	n.a.
S_1–Mo_1–Mo_2–S_2	154	157	154	153	165	154	165
R–C_1–C_2–R	n.a.		0	2	8	10	n.a.

n.a.: not applicable.

than the corresponding distances with the molybdenum atom bearing the terminal disulfide ligand. The Mo–O distance to the tricoordinated molybdenum atom was lengthened but only by 0.04 Å. Although many compounds comprising this core exist, they all entail identical ligands [12]; a distortion of the *syn*-[$Mo_2(O)_2(\mu\text{-}S)_2$] core consistently found by crystallographic analyses and molecular calculations on the side of the Mo atom bearing the terminal disulfide ligand is a new phenomenon that could participate in the non-symmetric behaviour of these compounds in the gas phase.

3.3.2. ELF calculations

In order to relate these geometrical changes to an evolution of bonding properties, topological analyses of the electronic domains using the electron localisation function were carried out. The ELF topological analysis [13] provides a partition of the molecular space in different localization domains called basins [23], which are consistent with the assumptions of Lewis theory. Indeed, chemists' intuitive vision of bonding in molecules implicitly assumes a partition of space into adjacent regions corresponding to chemically meaningful entities such as atomic cores, bonds, and lone pairs. The aim of the topological approach of the chemical bond is the determination of such regions and of their boundaries with the help of rigorous mathematical tools.

Becke and Edgecombe's ELF function [24], noted $\eta(r)$, is derived from a measure of the pairing of electrons, a corner stone in all bonding theories. It is confined within the [0, 1] interval and tends to 1 where parallel spins are highly improbable (for example inside a lone pair or a bond region), whereas it is close to 0 near the boundaries of the electronic domains where parallel spin electrons are compelled to come close one another.

Graphical representations (Fig. 7) of the bonding can be obtained by plotting isosurfaces of the $\eta(r)$ function. Among the electronic domains thus defined one distinguishes core basins (termed C (atom)), which are located immediately around the nucleus and valence basins (termed V (list of atoms)), which fill the remaining space. Valence basins are characterised by their synaptic order [25], which is the number of core to which they are connected. Monosynaptic basins correspond to lone pair regions and di- or polysynaptic basins correspond to bonding regions.

The mean population of each region $\bar{N}_i$ can be obtained by integrating the electron density $\rho(r)$ of a given basin. A measure of the mean deviation of this population, or more physically, of the delocalisation, is given by the variance of the population:

$$\sigma^2(\bar{N}_i) = \left\langle N_i^2 \right\rangle - \langle N_i \rangle^2$$

The relative fluctuation of basin population:

$$\lambda(\bar{N}_i) = \frac{\sigma^2(\bar{N}_i)}{\bar{N}_i}$$

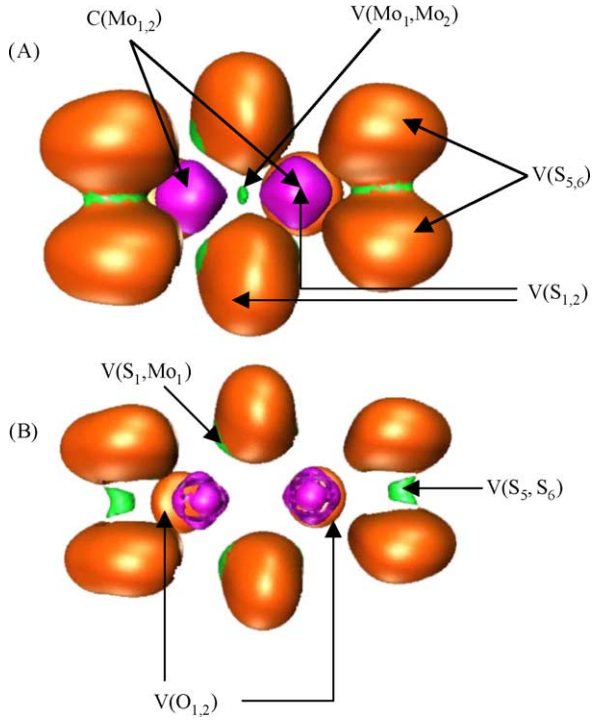

Fig. 7. Localisation domains for **1** (A) $\eta(r) = 0.45$ and (B) $\eta(r) = 0.75$. Colour code is as follows: magenta, core; orange brown, valence monosynaptic; green, valence disynaptic. (For interpretation of the references to colour in this figure legend, the reader is referred to the web version of the article.)

is a positive number expected to be less than 1 in most cases. A relative fluctuation larger than 0.45 is thought to indicate significant delocalisation [26].

The ELF basins provide a complementary view to the standard valence one. Instead of counting the atoms coordinated to a given nucleus, one is immersed in the basin of interest and counts the bordering cores. Therefore, we thought that such a population analysis, which implicitly takes into account the superposition of the resonance forms, could provide information on the origin of chemical properties and mechanisms of fragmentation.

The results of ELF calculations for anions **1**, **2**, **3** and $Mo_2S_4O_2^-$ are collected in Tables 3 and 4.

For all compounds, bonds were found to be quite weak as the population of shared electrons in di- or polysynaptic basins were all very low. This suggested a largely ionic cohesion. This, however, was not consistent with either the chemical properties [27] or the mass spectrometric behaviour which testify for a strong [$Mo_2(O)_2(\mu\text{-}S)_2$] core. A disynaptic valence basin between the two Mo atoms could be found, thus confirming the presence of a metal–metal bond, but its population of only about 0.4 electrons could not explain the strength of the dinuclear core entity. A better look at the data for **1**, however, allowed to delineate three modes of interaction which allow the cohesion of the [$Mo_2(O)_2(\mu\text{-}S)_2$] core and which are common to the four anions under study. These three cohesion factors have been observed before for other di- and trinuclear metal complexes [28]. The first and fore-

Table 3
Atoms in molecules (AIM) population analysis (number of electrons)

	Mo_1	Mo_2	O_1	O_2	S_3, S_4	S_1,S_2	S_5, S_6
$[Mo_2(O)_2\ (\mu\text{-}S)_2(\eta^2\text{-}S_2)_2]^{2-}$ **1**	40.43	40.43	8.80	8.80	16.47	16.71	16.48
$[Mo_2(O)_2(\mu\text{-}S)_2(\eta^2\text{-}S_2)\ (\eta^2\text{-}S_2C_2H_2)]^{2-}$ **2**	40.41	40.45	8.80	8.79	16.47	16.69	16.32
$[Mo_2(O)_2(\mu\text{-}S)_2(\eta^2\text{-}S_2)(\eta^2\text{-}S_2C_2(C_6H_5)_2)]^{2-}$ **3**	40.44	40.44	8.79	8.78	16.46	16.69	16.29
$Mo_2S_4O_2^-$	40.44	40.66	8.79	8.84	16.39	16.65	n.a.
$[Mo_2(O)_2(\mu\text{-}S)_2\ (\eta^2\text{-}S_2C_2H_2)]^-$	40.57	40.45	8.84	8.76	n.a.	16.70	16.29
$[Mo_2(O)_2(\mu\text{-}S)_2\ (\eta^2\text{-}S_2C_2(C_6H_5)_2)]^-$	40.70	40.42	8.78	8.75	n.a.	16.65	16.29
MoS_3O^-	40.46	n.a.	8.86	n.a.	16.43	(S_1) 16.74	n.a.

n.a.: not applicable.

most cohesion factor may be imputed to bridging sulphur atoms whose valence basins V(S_1) and V(S_2) (which will be further referred to as V($S_{1,2}$) as they are strictly identical) appeared at first as largely monosynaptic but are in fact characterised by an unusual relative fluctuation of 0.35 for the 5.53 electrons involved. This fluctuation can be translated in terms of a large delocalisation of the corresponding population, which is spread between the valence and core basins of the two molybdenum atoms. This confirmed the presence of a strong Mo–S as originally suggested and evidenced by Spivack and Dori [29]. This delocalisation was also partly true for the seven electrons of the terminal oxygen basins V(Mo_1,O_1) and V(Mo_2,O_2). The second and less important cohesion factor is the disynaptic valence basin between the two Mo atoms V(Mo_1,Mo_2). Its population of 0.4 electrons is accompanied by a considerable relative fluctuation of 0.90, which indicates a large delocalisation of this already low population on the bridging sulphurs and terminal oxygen atoms. Finally, a third cohesion factor may be imputed to a resonance between the core basins C(Mo) of the molybdenum atoms, attested by the high value of variance ($\sigma^2 = 2.45$) for both domains. The Mo core population C(Mo) are about 39 indicating an average Mo(III) oxidation state rather than Mo(V), which is the formal oxidation state assigned to Mo in this system. This situation is normal as formal oxidation states and calculated charges are rarely similar [30] and in fact +5 charges are almost never encountered in theoretical representation of transition metal complexes [31]. This uneven core population however is inconsistent with the low spin singlet state of the complex and the absence of spin polarization. In fact, because the metal dimer is in a closed-shell singlet state, each metallic core can be considered as a local closed-shell subsystem [26]. Taking this into consideration along with the resulting Mo(III) average oxidation state, only resonance between several even core configurations are compatible. Here, we will adopt a [Kr]c^n notation for the electronic core configuration of the metal atoms in the anions. [Kr] denotes the 18 electron pairs of the core, and c^n the extra electrons localized within the core basin that correspond to d electrons. With this notation, the compatible resonant core configurations would be [Kr]$c^2 \leftrightarrow$ [Kr]c^4, [Kr]$c^4 \leftrightarrow$ [Kr]c^2 or [Kr]$c^6 \leftrightarrow$ [Kr]c^0, [Kr]$c^0 \leftrightarrow$ [Kr]c^6. Knowing the first two configurations would contribute 1 to the standard deviation σ and the other two configurations 3, the value 2.45 for the variance σ^2 can be recovered by considering the two configurations should both contribute with a weight factor of 72% for Mo_1[Kr]$c^2 \leftrightarrow$ [Kr]c^4, [Kr]$c^4 \leftrightarrow$ [Kr]c^2 and 28% for [Kr]$c^6 \leftrightarrow$ [Kr]c^0, [Kr]$c^0 \leftrightarrow$ [Kr]c^6 [32]. The overlap between "d" orbitals generally thought to be responsible of the metal–metal bond in molecular orbital theory has been substituted in the ELF topological description by the concept of delocalisation of the core electrons and the formation of disynaptic intermetallic valence basins. While this last aspect has been related to the concentration of electron density due to orbital overlaps, the concept of electron density delocalisation between core basins has no analog in molecular orbital

Table 4
Mean electronic population $\bar{N}_i$ of the valence basins (number of electrons) with the relative fluctuation $\lambda(\bar{N}_i)$ indicated in parenthesis

	$Mo_2S_6O_2^{2-}$ 1	$Mo_2S_6O_2C_2H_2^{2-}$ 2	3	$Mo_2S_4O_2^-$	$Mo_2S_4O_2\ C_2H_2^-$	$Mo_2S_4O_2\ C_2(C_6H_5)_2^-$	MoS_3O^-
V(Mo_1,Mo_2)	0.42 (0.90)	0.39 (0.90)	0.39 (0.90)	0.45 (0.90)	0.42 (0.90)	0.42 (0.90)	n.a.
V(Mo_1,$S_{1,2}$)	0.88 (0.77)	0.85 (0.87)	0.89 (0.76)	1.37 (0.69)	1.12 (0.73)	1.12 (0.73)	4.01 (0.45)
V(Mo_2,$S_{1,2}$)	0.90 (0.77)	*	*	0.98 (0.77)	*	*	n.a.
V(Mo_1,$S_{3,4}$)	0.66 (0.80)	0.66 (0.81)	0.63 (0.81)	*	n.a.	n.a.	*
V(Mo_2,$S_{5,6}$)	0.67 (0.80)	1.35 (0.67)	1.45 (0.65)	n.a.	1.02 (0.73)	1.27 (0.68)	n.a.
V(S_3,S_4)	1.01 (0.85)	1.02 (0.85)	1.03 (0.85)	1.06 (0.72)	n.a.	n.a.	*
V(S_5,S_6)	1.02 (0.85)	*	*	n.a.	*	*	n.a.
V($S_{1,2}$)	5.54 (0.35)	6.44 (0.30)	6.39 (0.30)	4.95 (0.38)	6.26 (0.32)	5.50 (0.35)	3.30 (0.47)
V($S_{3,4}$)	5.49 (0.46)	5.48 (0.46)	5.51 (0.46)	6.70 (0.45)	n.a.	n.a.	6.67 (0.45)
V($S_{5,6}$)	5.49 (0.46)	4.44 (0.52)	4.32 (0.37)	n.a.	4.72 (0.51)	4.55 (0.51)	n.a.
V(Mo_1,O_1)	6.99 (0.20)	7.00 (0.20)	6.98 (0.20)	6.97 (0.20)	6.96 (0.21)	6.99 (0.21)	7.09 (0.20)
V(Mo_2,O_2)	7.01 (0.20)	6.99 (0.21)	6.99 (0.21)	7.06 (0.20)	7.06 (0.19)	7.00 (0.20)	n.a.

As the molecules are symmetric, sulphur atoms S_1 and S_2, S_3 and S_4, S_5 and S_6 show identical values and are thus referred to as $S_{1,2}$, $S_{3,4}$ and $S_{5,6}$. The asterisk (*) signal the disappearance of a valence basin compared to $Mo_2S_6O_2^{2-}$, by a shift of the corresponding electron population to other domains; n.a.: not applicable; *valence population transferred.

theory. The resonance between even core configurations also confirmed the link between the diamagnetism of the complex and the presence of a strong Mo–Mo interaction suggested by Spivack and Dori [29].

This largely delocalised character of electrons from the bridging sulphur, terminal oxygen and molybdenum atoms could be found in all four computed structures and only minor differences could be observed. In fact, the addition of the organic group to form the dithiolene ligands was found to induce only a few changes in the electronic population of the different atoms in the anion as might be observed in Table 3. Table 4 shows that one change generated by the organic group is a transfer of 0.90 electron from the disynaptic basin between one of the molybdenum atom and the bridging sulphur atoms V(Mo_2, $S_{1,2}$) to the valence basin between the Mo atom and the dithiolene sulphurs V(Mo_2, $S_{5,6}$) This transfer is associated with a slight decrease of the electronic population in the disynaptic basin V(Mo_1,Mo_2), as well as in the monosynaptic basins of the dithiolene sulphurs V($S_{5,6}$), the effect being a little larger for diphenyl acetylene than for acetylene as expected from its larger electronic withdrawing property. Notably, the population of the monosynaptic valence basin V($S_{1,2}$) on the bridging sulfido groups are increased.

Upon fragmentation to $Mo_2S_4O_2^-$ the evolution of the electron localization could be described as follows: (i) a slight increase of the electronic population on the tricoordinated Mo atom (Mo_2) associated with a corresponding decrease on all sulphur atoms (Table 3); (ii) an increase of the population in the disynaptic basins between the molybdenum and the bridging sulfido groups V(Mo_1,$S_{1,2}$), V(Mo_2,$S_{1,2}$) and a decrease of the electronic density corresponding to the lone pairs of the same bridging sulfido groups V($S_{1,2}$) and (iii) an increase in the population of the terminal η^2 disulfide V($S_{3,4}$).

The overall effect of the fragmentation was therefore to shift the electron density towards the terminal disulfide S_3–S_4 and to slightly reduce the Mo_2 atom, which undergoes a diminution of its coordination sphere. These phenomena occur with the minimal structural alteration, in consistency with the least topological change principle. In fact, this principle could account for the non-symmetrical fragmentation behaviour of **2** and **3**.

Indeed, the relative energy of computed structures could not explain the fragmentations as DFT calculations on the energy for the dissociation of S_2^- or even the cleavage of the metal–metal bond led to similar or lower energies. ELF calculations on the unobserved fragment ions $[Mo_2(O)_2(\mu\text{–}S)_2(\eta^{2-}S_2C_2(C_6H_5)_2)]^-$ and $[Mo_2(O)_2(\mu\text{-}S)_2(\eta^2\text{-}S_2C_2H_2)]^-$ showed that the loss of a S_2^- group from complexes **2** and **3** would result in a shift of the electron density towards that remaining dithiolene ligand and a slight reduction of the tricoordinated Mo_1 atom. This shift, however, would involve a lower electronic population in all disynaptic basins, this population being transferred to the monosynaptic basins of the bridging sulphurs V($S_{1,2}$) and dithiolene sulphurs V($S_{5,6}$). The overall electronic delocalisation over the $[Mo_2(O)_2(\mu\text{-}S)_2]$ core would thus be decreased, inducing a larger topological change. Cleavage of the metal–metal bond to the fragment ion MoS_3O^- would also induce large topological changes as attested by the values in Table 4.

4. Conclusion

The gas phase fragmentations of a family of three anionic complexes of molybdenum(V), $[Mo_2(O)_2(\mu\text{-}S)_2(\eta^2\text{-}S_2)_2]^{2-}$, $[Mo_2(O)_2(\mu\text{-}S)_2(\eta^2\text{-}S_2)\ (\eta^2\text{-}S_2C_2H_2)]^{2-}$, $[Mo_2(O)_2(\mu\text{-}S)_2(\eta^2\text{-}S_2)(\eta^2\text{-}S_2C_2(C_6H_5)_2)]^{2-}$ were studied as a function of the collision energy used in the collision cell of a triple quadrupole analyser. The main fragment ion for the three anions was $Mo_2S_4O_2^-$ at low collision energies, while higher collisional activation lead to cleavage of the metal–metal bond. Addition of organic groups to form dithiolene ligands lead to slightly increased dissociation energy. Topological analyses of the electronic domains using the electron localisation function showed three cohesive factors could account for the strength of the dinuclear core: (i) a significant resonance of the core electrons of the two Mo atoms, (ii) a delocalisation of the electrons on the bridging sulfido groups and terminal oxygen atoms and finally (iii) the presence of a small and highly delocalised electron population in a disynaptic valence basin between the Mo atoms.

The non-symmetric fragmentation behaviour could be interpreted with the least topological change principle. Fragmentation induced a shift of the electron density towards the remaining ligands and a slight increase of the electron population on the Mo atom that undergoes a diminution of its coordination sphere. We expect this reduction of the metallic center to continue with the loss of other ligands. Electron localization function calculations are underway to confirm and characterise the reduction process accompanying further dissociation reactions.

Acknowledgements

These computations have been performed at the Centre de Ressources Informatiques de Haute-Normandie (CRIHAN, Saint Etienne Du Rouvray) within the frameworks of the “Bassin Parisien Régional Plan” (CPIBP) local modeling center for engineering sciences contract (article 12) and of the “Réseau Normand pour la Modélisation Moléculaire”, at the Centre de Calcul pour la Recherche (CCR, Univ. P. & M. Curie). We are pleased to thank Mme Claude Giessner-Prettre and Mr. Bernard Silvi for helpful discussions and suggestions and Claudine Keil for her help and technical support. We also wish to acknowledge the Région Ile de France for a Sesame financial support concerning the API3000.

References

[1] (a) M. Yamashita, J.B. Fenn, J. Phys. Chem. 88 (1984) 4451;
(b) M. Yamashita, J.B. Fenn, J. Phys. Chem. 88 (1984) 4671;
(c) R. Colton, J.C. Traeger, Inorg. Chim. Acta 201 (1992) 153;
(d) J.C. Traeger, Mass Spectrom. Rev. 14 (1995) 79;
(e) I.I. Stewart, G. Horlick, Trends Anal. Chem. 75 (1996) 80;
(f) C.L. Gatlin, F. Turecek, in: R.B. Cole (Ed.), Electrospray Ionization Mass Spectrometry, John Wiley & Sons, New York, 1997, p. 527;
(g) J.C. Traeger, Int. J. Mass Spectrom. 200 (2000) 387.

[2] (a) V. Katta, S.K. Chowdhury, B.T. Chait, J. Am. Chem. Soc. 112 (1990) 5348;
(b) A. Karaliota, L.V. Aletras, D. Hatzipanayioti, J. Mass Spectrom. 37 (2002) 760.

[3] G.J. Van Berkel, J.M. Quirke, R.A. Tigani, A.S. Dilley, T.R. Covey, Anal Chem. 70 (1998) 1544.

[4] G.A. Khitrov, G.F. Strouse, J.J. Gaumet, J. Am. Soc. Mass Spectrom. 15 (2004) 260.

[5] C. Moucheron, A. Kirsch-De Mesmaeker, A. Dupont-Gervais, E. Leize, A. Van Dorsselaer, J. Am. Chem. Soc. 118 (1996) 12834.

[6] (a) C. Jiang, T.S.A. Hor, Y.K. Yan, W. Henderson, L.J. McCaffrey, J. Chem. Comm. Dalton Trans. 18. (2000) 3197;
(b) P.J. Dyson, A.K. Hearley, B.F.G. Johnson, J.S. McIndoe, P.R.R. Langridge-Smith, C. Whyte, Rap. Commun. Mass Spectrom. 15 (2001) 895;
(c) P.J. Dyson, J.S. McIndoe, Inorg. Chim. Acta 354 (2003) 68;
(d) P. Dalgaard, C.J. Mckenzie, J. Mass Spectrom. 34 (1999) 1033.

[7] R. Hille, Chem. Rev. 96 (1996) 2757.

[8] F.A. Cotton, Multiple Bonds Between Metal Atoms, second ed., Oxford University Press, Oxford, 1993.

[9] F.A. Cotton, Inorg. Chem. 37 (1998) 5710.

[10] R. Dessapt, C. Simonnet-Jégat, A. Mallard, H. Lavanant, J. Marrot, F. Sécheresse, Inorg. Chem. 42 (2003) 6425.

[11] R. Dessapt, C. Simonnet-Jégat, J. Marrot, F. Sécheresse, Inorg. Chem. 40 (2001) 4072.

[12] T. Shibahara, Coord. Chem. Rev. 123 (1993) 73.

[13] (a) B. Silvi, A. Savin, Nature 371 (1994) 683;
(b) A. Savin, B. Silvi, F. Colonna, Can. J. Chem. 74 (1996) 1088;
(c) For a review, see: A. Savin, R. Nesper, S. Wengert, T.F. Fässler, Angew. Chem. Int. Ed. Eng. 36 (1997) 1808.

[14] GAUSSIAN 98 (Revision A5), M.J. Frisch, G.W. Trucks, H.B. Schlegel, G.E. Scuseria, M.A. Robb, J.R. Cheeseman, V.G. Zakrzewfki, J.A. Montgomery, R.E. Stratmann, J.C. Burant, S. Dapprich, J.M. Millam, A.D. Daniels, K.N. Kudin, M.C. Strain, O. Farkas, J. Tomasi, V. Barone, M. Cossi, R. Cammi, B. Mennucci, C. Pomelli, C. Adamo, F. Clifford, J. Ochterski, G.A. Petersson, P.Y. Ayala, Q. Cui, K. Morokuma, D.K. Malick, A.D. Rabuck, K. Raghavachari, J.B. Foresman, J. Cioslowski, J.V. Ortiz, B.B. Stefanov, G. Liu, A. Liashenko, P. Piskorz, I. Komaromi, R. Gomperts, R.L. Martin, D.J. Fox, T. Keith, M.A. Al-Laham, C.Y. Peng, A. Nanayakkara, C. Gonzalez, M. Challacombe, P.M.W. Gill, B.G. Johnson, W. Chen, M.W. Wong, J.L. Andres, M. Head-Gordon, E. S. Replogle, J.A. Pople, Gaussian Inc., Pittsburgh, PA, 1998.

[15] A.D. Becke, J. Chem. Phys. 98 (1993) 5648.

[16] C. Lee, Y. Yang, R.G. Parr, Phys. Rev. B 37 (1988) 785.

[17] (a) F.A. Cotton, X. Feng, J. Am. Chem. Soc. 119 (1997) 7514;
(b) F.A. Cotton, X. Feng, J. Am. Chem. Soc. 120 (1998) 3387;
(c) I. Demachy, A. Lledos, Y. Jean, Inorg. Chem. 38 (1999) 5443.

[18] EMSL basis set library, http://www.emsl.pnl.gov/.

[19] (a) S. Noury, X. Krokidis, F. Fuster, B. Silvi, TopMod Package; Paris, 1997;
(b) S. Noury, X. Krokidis, F. Fuster, B. Silvi, Comput. Chem. 23 (1999) 597.

[20] E. Pepke, J. Murray, J. Lyons, T.-Z. Hwu, Scian, Supercomputer Computations Research Institute, Florida State University, Tallahassee, FL, 1993.

[21] (a) H. Lavanant, H. Virelizier, Y. Hoppilliard, J. Am. Soc. Mass Spectrom. 9 (1998) 1217;
(b) H. Lavanant, E. Hecquet, Y. Hoppilliard, Int. J. Mass Spectrom. Ion Process 185/186/187 (1999) 11;
(c) I.K. Chu, C.F. Rodriguez, A.C. Hopkinson, K.W.M. Siu, T.C. Lau, J. Am. Soc. Mass Spectrom. 12 (2001) 1114;
(d) S. Wee, R.A.J. O'Hair, W.D. McFayden, Rap. Commun. Mass Spectrom. 16 (2002) 884.

[22] T. Waters, S.J. Blanksby, L. Zhang, R.A.J. O'Hair, Org. Biomol. Chem. 2 (2004) 190.

[23] R.F.W. Bader, Atoms in Molecules: A Quantum Theory, Oxford University Press, London, 1990.

[24] A.D. Becke, K.E. Edgecombe, J. Chem. Phys. 92 (1990) 5397.

[25] X. Krokidis, S. Noury, B. Silvi, J. Phys. Chem. A 101 (1997) 7277.

[26] A. Savin, B. Silvi, F. Colonna, Can. J. Chem. 74 (1996) 1088.

[27] (a) D. Coucouvanis, A. Toupadakis, S.M. Koo, C.G. Kim, A. Hadjikyriacou, J. Am. Chem. Soc. 113 (1991) 5271;
(b) R. Bhattacharayya, P.K. Chakrabarty, P.N. Ghosh, A.K. Mukherjee, D. Podder, M. Mukherjee, Inorg. Chem. 30 (1991) 3948;
(c) A. Mederos, D.M. Saysell, J. Sanchiz, A.G. Sykes, J. Chem. Soc., Dalton Trans. (1998) 2723;
(d) E. Cadot, F. Sécheresse, Chem. Commun. (2002) 2189.

[28] (a) M. Féliz, R. Llusar, J. Andrès, S. Berski, B. Silvi, New J. Chem. 26 (2002) 844;
(b) R. Llusar, J. Beltrán, F. Fuster, B. Silvi, J. Phys. Chem. A 105 (2001) 9460.

[29] (a) B. Spivack, Z. Dori, J. Chem. Soc., Chem. Commun. (1973) 909;
(b) B. Spivack, Z. Dori, J. Chem. Soc., Dalton Trans. (1973) 1173.

[30] M.M. Rohmer, M. Bernard, Inorg. Chem. 41 (2002) 892.

[31] T. Wagener, G. Frenking, Inorg. Chem. 37 (1998) 1805.

[32] B. Silvi, Personal Communication.